EUROPEAN ORGANIZATION FOR NUCLEAR RESEARCH
European Laboratory for Particle Physics

Large Hadron Collider Project

LHC Project Report 446

INTEGRATED DESIGN OF SUPERCONDUCTING MAGNETS WITH THE CERN FIELD COMPUTATION PROGRAM ROXIE

S. Russenschuck, M. Aleksa, M. Bazan, J. Lucas, S. Ramberger and C. Völlinger

Abstract

The program package ROXIE has been developed at CERN for the field computation of superconducting accelerator magnets and is used as an approach towards the integrated design of such magnets. It is also an example of fruitful international collaborations in software development.The integrated design of magnets includes feature based geometry generation, conceptual design using genetic optimization algorithms, optimization of the iron yoke (both in 2d and 3d) using deterministic methods, end-spacer design and inverse field calculation.The paper describes the version 8.0 of ROXIE which comprises an automatic mesh generator, an hysteresis model for the magnetization in superconducting filaments, the BEM-FEM coupling method for the 3d field calculation, a routine for the calculation of the peak temperature during a quench and neural network approximations of the objective function for the speed-up of optimization algorithms, amongst others.New results of the magnet design work for the LHC are given as examples.

LHC-ICP

Presented at the 6th International Conference on Computational Accelerator Physics
Darmstadt, Germany, 11-14 September 2000, Darmstadt, Germany

Administrative Secretariat
LHC Division
CERN
CH - 1211 Geneva 23
Switzerland

Geneva, 15 December 2000

Integrated Design of Superconducting Magnets with the CERN Field Computation Program ROXIE

S. Russenschuck, M. Aleksa, M. Bazan, J. Lucas, S. Ramberger, C. Völlinger
CERN, 1211 Geneva 23, Switzerland

The program package ROXIE has been developed at CERN for the field computation of superconducting accelerator magnets and is used as an approach towards the integrated design of such magnets. It is also an example of fruitful international collaborations in software development. The integrated design of magnets includes feature based geometry generation, conceptual design using genetic optimization algorithms, optimization of the iron yoke (both in 2d and 3d) using deterministic methods, end-spacer design and inverse field calculation. The paper describes the version 8.0 of ROXIE which comprises an automatic mesh generator, an hysteresis model for the magnetization in superconducting filaments, the BEM-FEM coupling method for the 3d field calculation, a routine for the calculation of the peak temperature during a quench and neural network approximations of the objective function for the speed-up of optimization algorithms, amongst others. New results of the magnet design work for the LHC are given as examples.

I. INTRODUCTION

The design and optimization of the superconducting (SC) magnets for the LHC are dominated by the requirement of an extremely uniform field, which is mainly defined by the layout of the superconducting coils. Even very small geometrical effects such as the insufficient keystoning of the cable (cable inner and outer diameter not following curvatures of circles), the insulation, grading of the current density in the cable due to different cable compaction and coil deformations due to collaring, cool down and electromagnetic forces have to be considered for the field calculation.

Therefore, the ROXIE (**R**outine for the **O**ptimization of magnet **X**-sections, **I**nverse field calculation and coil **E**nd design) program package was developed at CERN for the design and optimization of the LHC SC magnets. It is now also more and more applied in institutes outside CERN. In collaboration with the Technical University of Graz, Austria, the program was extended to include the calculation of iron saturation effects using a reduced vector-potential method. ROXIE also includes the method of coupled boundary / finite-elements (BEM-FEM), which was developed at the University of Stuttgart, Germany, and which is specially suited for the calculation of 3-dimensional effects in the magnets. The advantage of both methods is that the coils do not need to be represented in the finite-element mesh and can therefore be modeled with the required accuracy.

The development of the program was driven by four main objectives:

- To write an easy-to-use program for the design of SC coils in two and three dimensions considering field quality, quench margin and persistent current multipoles arising from the SC magnetization.
- To include the program into a mathematical optimization environment for field optimization and inverse problem solving.
- To provide for field computation techniques specially suited for SC magnets.
- To develop an integrated design tool with sophisticated graphic routines and interfaces to CAD-CAM systems for the making of drawings and the manufacture of coil end-spacers.

The main improvements in the ROXIE 8.0 version with respect to older version (described, e.g., in [33]) are:

- Interface to the BEM-FEM coupling method for the calculation of iron magnetization both in 2d and 3d.
- Automatic mesh generator for quadrilateral meshes based on a domain decomposition method.
- A Hysteresis model for superconducting filaments coupled to the FEM and BEM-FEM method, with a M(B)-iteration for the consideration of arbitrarily shaped iron yokes.
- Analytical model for the calculation of quench-currents and peak temperatures for long magnets with heaters (no propagation effects).
- Axisymmetric geometries (Solenoids) with or without iron yoke.
- Permanent magnet excitation.
- Automated install routines for UNIX systems.
- Optimization algorithm EXTREM with a neural network approximator for speedup of the optimization process.
- Post processing for magnetic levitation devices.
- Virtual reality interface for coil-end geometries.

II. FIELD QUALITY IN ACCELERATOR MAGNETS

The quality of the magnetic field is essential to keep the particles on stable trajectories. The magnetic field errors in the aperture of the magnets are expressed as the coefficients of the Fourier-series expansion of the radial field component at a given reference radius (in the 2-dimensional case). In the 3-dimensional case, the transverse field components are given at a longitudinal position z_0 or integrated over the entire length of the magnet. Assuming that the radial component of the magnetic flux density B_r at a given reference radius $r = r_0$ inside the aperture of a magnet is measured or calculated as a function of the angular position φ we get for the Fourier-series expansion of the field

$$B_r = \sum_{n=1}^{\infty}(B_n \sin n\varphi + A_n \cos n\varphi) = B_N \sum_{n=1}^{\infty}(b_n \sin n\varphi + a_n \cos n\varphi). \quad (1)$$

The field components are related to the main field component B_N ($N = 1$ dipole, $N = 2$ quadrupole, etc.). The B_n are called the *normal* and the A_n the *skew* components of the field given in Tesla, b_n the normal relative, and a_n the skew relative field components. They are dimensionless and are usually given in units of 10^{-4} at a 17 mm reference radius.

Let us consider a single coil centered in an iron yoke with circular inner aperture and a uniform, high permeability. The coil can be accurately described by a set of line-currents at the position of the SC strands. For a set of n_s individual line-currents at the position (r_i, Θ_i) carrying a current I_i, the coefficients are given by

$$B_n = -\sum_{i=1}^{n_\mathrm{s}} \frac{\mu_0 I_i}{2\pi} \frac{r_0^{n-1}}{r_i^n} \left(1 + f_\mu (\frac{r_i}{R_\mathrm{yoke}})^{2n}\right) \cos n\Theta_i, \quad (2)$$

$$A_n = \sum_{i=1}^{n_\mathrm{s}} \frac{\mu_0 I_i}{2\pi} \frac{r_0^{n-1}}{r_i^n} \left(1 + f_\mu (\frac{r_i}{R_\mathrm{yoke}})^{2n}\right) \sin n\Theta_i, \quad (3)$$

at a given reference radius r_0 where the factor f_μ is given as

$$f_\mu = \frac{\mu_\mathrm{r} - 1}{\mu_\mathrm{r} + 1}. \quad (4)$$

R_yoke is the inner radius of the iron yoke with the relative permeability μ_r. As SC cables are composed of single strands with a diameter of about 1 mm, a good computational accuracy can be obtained by representing each cable by two layers of equally spaced line-currents at the strand position. Thus the grading of the current density in the cable due to the different compaction on its narrow and wide side is automatically considered.

With equations (2) and (3), a semi-analytical method for calculating the fields in SC magnets is given. The iron yoke is represented by image currents (the second term in the parentheses). At low field level, when the saturation of the iron yoke is low, this is a sufficient method for optimizing the coil cross-section.

The relative contribution of the iron yoke to the total field (coil field plus iron magnetization) is for a non-saturated yoke ($\mu_\mathrm{r} \gg 1$) approximately $(1+(\frac{R_\mathrm{yoke}}{r})^{2n})^{-1}$. For the main dipoles (with a mean coil radius of $r =$ 43.5 mm and a yoke radius of $R_\mathrm{yoke} = 89$ mm) we get a 19% yoke contribution to the B_1 component, whereas for the B_5 component the influence of the yoke is only 0.07%.

It is therefore appropriate to optimize for higher harmonics first using analytical field calculation, and calculate the effect of iron saturation on the lower-order multipoles only at a later stage. When the LHC dipole magnets are ramped to their nominal field of 8.33 T in the aperture, the yoke is highly saturated, and numerical methods have to be used to replace the imaging method. In this case it is advantageous to use numerical methods that allow a distinction between the coil-field and the iron magnetization effects, to confine both modeling problems on the coils and FEM-related numerical errors to the 20% of field contribution from the iron magnetization. Collaborative efforts with the University of Graz, Austria, and the University of Stuttgart, Germany, have been undertaken for this task. Both the method of reduced vector-potentials as well as the BEM-FEM coupling method yields the reduced field in the aperture caused by the magnetization of the iron yoke and avoids the representation of the coil in the FE-meshes.

III. COIL MODELER

Coil cross sections and ends of accelerator magnets made of Rutherford type SC cables are generated from only a few meaningful engineering data such as the number of conductors per block, conductor type, radius of the winding mandrel and the positioning and inclination angles of the blocks. Different coil block arrangements can be modeled.

- So-called $\cos\Theta$ coils with alignment of the conductors on the inner diameter, i.e., the shape of the coil being determined by the winding mandrel and the curing mold.
- $\cos\Theta$ coils with alignment on the outer diameter, i.e., the shape is determined by the coil outer and the collar inner diameter,respectively.
- Window frame coils with rectangular coil blocks.
- Axi-symmetric coils (solenoids).

The input parameters for the coil-end modeling are the z-position of the first conductor of each coil block, its inclination angle in the yz plane, the straight section and the size of inter turn wedges between the conductors. Four options are available:

- Constant perimeter coil-ends with inter-turn wedges and conductors placed on the winding mandrel.
- Grouped conductors aligned at the outer radius, featuring end-spacers with shelfs.
- Coil-ends for magnets with rectangular cross sections.
- Racetrack coil ends, with or without additional straight section, suited for the modeling of solenoids, wigglers and torus magnets.

The geometric positions of conductors can be printed in different formats suitable for other numerical field calculation packages such as ANSYS and OPERA as well as in a DXF format. The form of the end spacers can be generated automatically and the polygons describing the surfaces can be transferred into CAD-CAM systems for the machining of these pieces using 5 axis milling machines or 5 axis water-jet cutters.

All the input data necessary for the coil modeling can be defined as design variables and are automatically updated during the optimization process.

Fig. 1 shows the ROXIE model of the LHC main dipole extremity, with an inner (non-magnetic) ring in the yoke in order to reduce the peak field in the coil ends with their weaker mechanical structure.

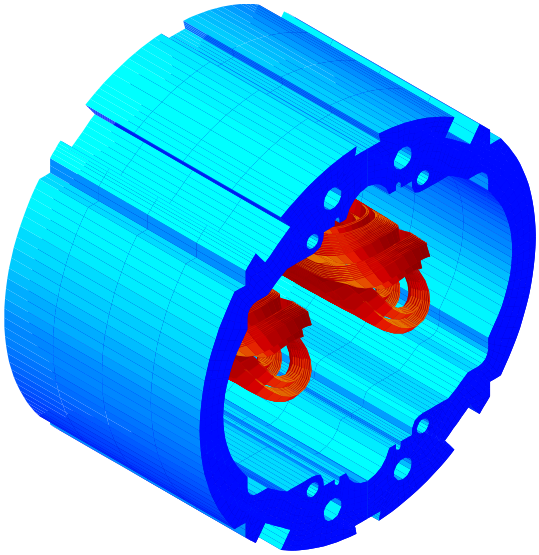

FIG. 1. ROXIE model of the LHC main dipole extremities.

IV. YOKE MODELER AND MESH-GENERATOR

The yoke modeler allows the definition of symbols which can then be used for the definition of key-points in the finite-element domain. Yoke modeler, mesh generator and the finite element software are coupled through transfer files to keep the size of the executable within 250 MB. If optimization algorithms are used, a transfer file contains the updated values of key-point data.

Simplex elements (triangles in 2D, tetrahedra in 3D) have the disadvantage that curved shapes can only be modeled by polygonal approximations. The advantage of a higher order approximation of the potentials may be lost due to a rather rough geometric approximation. An alternative are the *isoparametric* quadrilateral elements which have curved sides. Numerically unfavorable prisms can be avoided when the geometry is simply extruded into the third dimension. However, automatic mesh generators for these elements have only very recently been developed [37].

A new mesh generator based on geometrical domain decomposition, which was developed at the Mathematics Department of the University of Stuttgart, Germany [28] has been implemented in the ROXIE program package. The following extensions have been added.

- Extension of the method to 8 noded (higher order) quadrilateral elements.
- Parametric input for the definition of design variables for the mathematical optimization.
- Implementation of design modules for the definition of material boundaries.
- Feature based magnet modeling by means of the Gnu m4 macro language.
- A morphing algorithm for optimization and sensitivity studies which avoids re-meshing and changing mesh topologies during optimization.

The quadrilateral mesh generator implemented in ROXIE relies on the method of geometrical domain decomposition [28]. In a first step the area is decomposed into areas that are topologically equivalent to disks, i.e. holes are eliminated. This decomposition is continued until the remaining areas are regarded as “simple” (e.g. triangles or rectangles with up to 6 nodes on each side). These areas are then “filled” with quadrilaterals using a modified paving strategy [7]. In this approach an area gets “filled” from outside to the inside by adding full rows of rectangles. Finally, smoothing algorithms are applied to enlarge small angles and to reduce large angles, while leaving the mesh topology unchanged.

Since this mesh generator only produces finite-elements with 4 nodes, the middle points are added during the post processing and 8-noded (higher order)

quadrilateral elements are produced which are necessary for three dimensional BEM-FEM calculations.

Using the m4 macro language, magnetically relevant parts of the magnet (e.g. yoke, collar, inserts, cryostat, beam-screen etc.) can be modeled in different ".iron" files and can then be linked with the "include" command (notice that using the BEM-FEM method, disjunct iron parts can be separately meshed). It is also possible to re-use parametric models for different magnet variants (in particular for the MQ, MQM and MQY quadrupole magnets).

In order to make the new mesh generator applicable for optimization and sensitivity studies, a morphing technique known from computer graphics [6] was implemented [1].

Fig. 2 shows the quadrilateral finite element mesh in the yoke and collar of the insertion region quadrupole magnet MQM. Notice the disjunct finite-element domains, and the fact that the coil is not modeled in the mesh.

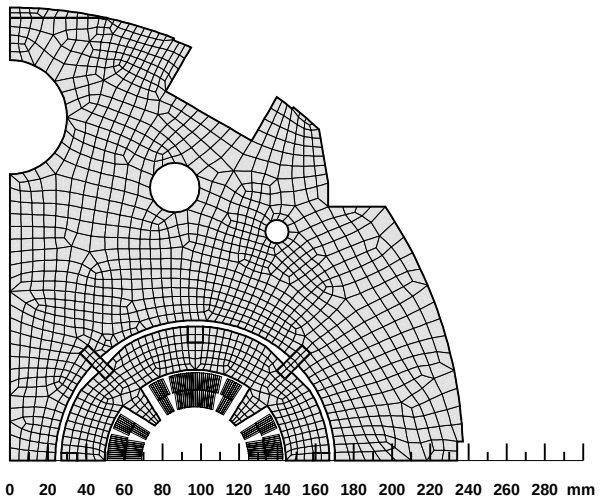

FIG. 2. Quadrilateral finite element mesh in the yoke and collar of the insertion region quadrupole magnet MQM

V. NUMERICAL FIELD CALCULATION

Magnets for particle accelerators have always been a key application of numerical methods in electromagnetism. Hornsby [19], in 1963, developed a code based on the finite difference method for the solving of elliptic partial differential equations and applied it to the design of magnets. Winslow [41] created the computer code TRIM (Triangular Mesh) with a discretization scheme based on an irregular grid of plane triangles by using a generalized finite difference scheme. He also introduced a variational principle and showed that the two approaches lead to the same result. In this respect, the work can be viewed as one of the earliest examples of the finite element method applied to the design of magnets. The POISSON code which was developed by Halbach and Holsinger [17] was the successor of this code and was still applied for the optimization of the SC magnets for the LHC during the early design stages.

Nevertheless, for the SC magnet design, it was necessary to find more appropriate formulations which do not require the modeling of the coils in the finite-element mesh. The program FEM2D, developed at the University of Graz, Austria, by Bardi, Biro, and Preis, includes a reduced vector-potential formulation, which is linked to the ROXIE code.

The vector-potential $\mathbf{A}$ is split into two parts:

$$\mathbf{A} = \mathbf{A}_\mathrm{s} + \mathbf{A}_\mathrm{r} \tag{5}$$

where $\mathbf{A}_\mathrm{r}$ is the reduced vector-potential due to the iron magnetization and $\mathbf{A}_\mathrm{s}$ is the impressed vector potential due to the source currents in free space. Accordingly

$$\mathbf{B} = \mu_0 \mathbf{H}_\mathrm{s} + \mathrm{curl}\mathbf{A}_\mathrm{r}. \tag{6}$$

The source vector potential can be calculated with Biot-Savart-type integrals. The weak integral form reads:

$$\int_\Omega \mathrm{curl}\mathbf{w}_\mathrm{a} \cdot \frac{1}{\mu}\mathrm{curl}\mathbf{A}_\mathrm{r}\,\mathrm{d}\Omega + \int_\Omega \mathrm{div}\mathbf{w}_\mathrm{a} \cdot \frac{1}{\mu}\mathrm{div}\mathbf{A}_\mathrm{r}\,\mathrm{d}\Omega = \int_\Omega \mathrm{curl}\mathbf{w}_\mathrm{a} \cdot (\mathbf{H}_\mathrm{s} - \frac{\mu_0}{\mu}\mathbf{H}_\mathrm{s})\,\mathrm{d}\Omega \tag{7}$$

with $a = 1, 2, 3$. In the air region $\mu = \mu_0$, and therefore the right hand side of eq. (7) is zero. The current density does not appear explicitly in the equation and the required source field in the iron region can be calculated by means of Biot-Savart's law.

Experience has shown that the influence of the far-field boundary on the multipoles is smaller using the reduced vector-potential formulation, since the reduced field accounts for only about 20 % of the total field and thus the error from the far-field boundary on the total field is reduced. Although the mesh in the air region does not have to model the coil, the air region must nevertheless be meshed. This is not a problem in the 2-dimensional calculations but proves troublesome in the 3D case.

Another problem in the 3D implementation is the fact that the solution to the vector boundary value problem is not unique. One method for overcoming this problem is the introduction of the so-called Coulomb gauge. However, the use of the gauged formulation with reduced vector-potential creates convergence problems, as the permeability jumps at the material boundaries between iron and air, and the interface condition for $\mathrm{div}\mathbf{A_r}$ on the boundary implies a large jump in the divergence of $\mathbf{A_r}$, a quantity which should be zero [8]. As the method of finite-elements ensures only the approximate satisfaction of the weak form, an error in the fulfillment of the Coulomb gauge is present and therefore $\mathrm{div}\mathbf{A_r} \neq 0$. Due to the interface condition, the error in the iron region is then even higher. In the 2D case the divergence of the vector-potential is zero and this problem does not appear.

A. BEM-FEM coupling method

The disadvantage of the finite-element method is that only a finite domain can be discretized, and therefore the field calculation in the magnet coil-ends with their large fringe-fields requires a large number of elements in the air region. The relatively new boundary-element method is defined on an infinite domain and can therefore solve open boundary problems without approximation with far-field boundaries. The disadvantage is that non-homogeneous materials are difficult to consider.

The method of coupled boundary-elements / finite-elements (BEM-FEM), developed by Fetzer, Haas, and Kurz at the University of Stuttgart, Germany, combines a FE description using incomplete quadratic (20-node) elements. The method relies on a gauged total vector-potential formulation for the interior of the magnetic parts, and a boundary element formulation for the coupling of these parts to the exterior, which includes excitational coil fields. This implies that the air regions need not to be meshed at all. Experience has shown that the gauged formulation is applicable for the field calculation of SC magnets.

The BEM-FEM method couples the finite-element method inside magnetic domains $\Omega_\mathrm{i} = \Omega_\mathrm{FEM}$ with the boundary-element method in the domain outside the magnetic material $\Omega_\mathrm{a} = \Omega_\mathrm{BEM}$, by means of the normal derivative of the vector-potential on the interface Γ_ai between iron and air. The application of the BEM-FEM method to magnet design has the following intrinsic advantages:

- The coil field can be taken into account in terms of its source vector potential $\mathbf{A}_\mathrm{s}$, which can be obtained easily from the filamentary currents I_s by means of Biot-Savart type integrals without the meshing of the coil.
- The BEM-FEM coupling method allows for the direct computation of the reduced vector potential $\mathbf{A}_\mathrm{r}$ instead of the total vector potential $\mathbf{A}$. Consequently, errors do not influence the dominating contribution $\mathbf{A}_\mathrm{s}$ due to the SC coil.
- Because the field in the aperture is calculated through the integration over all the BEM elements, local field errors in the iron yoke cancel out and the calculated multipole content is sufficiently accurate even for very sparse meshes.
- The surrounding air region need not be meshed at all. This simplifies the preprocessing and avoids artificial boundary conditions at some far-field-boundaries. Moreover, the geometry of the permeable parts can be modified without regard to the mesh in the surrounding air region, which strongly supports the feature based, parametric geometry modeling that is required for mathematical optimization.
- The method can be applied to both 2D and 3D field problems.

Inside the magnetic domain a gauged vector-potential formulation is applied.

$$\frac{1}{\mu_0}\mathrm{curl}\,\mathrm{curl}\mathbf{A} = \mathbf{J} + \mathrm{curl}\mathbf{M} \tag{8}$$

$$\frac{1}{\mu_0}(-\nabla^2\mathbf{A} + \mathrm{grad}\,\mathrm{div}\mathbf{A}) = \mathbf{J} + \mathrm{curl}\mathbf{M} \tag{9}$$

Using the Coulomb gauge $\mathrm{div}\mathbf{A} = 0$, forcing the weighted residual to zero, and applying Green's first theorem yields the weak integral form

$$\begin{aligned}\frac{1}{\mu_0}\int_{\Omega_\mathrm{i}} \mathrm{grad}(\mathbf{A}\cdot\mathbf{e}_\mathrm{a})\cdot\mathrm{gradw}_\mathrm{a}\,\mathrm{d}\Omega_\mathrm{i} \\ -\frac{1}{\mu_0}\oint_{\Gamma_\mathrm{ai}}\left(\frac{\partial\mathbf{A}}{\partial n_\mathrm{i}} - (\mu_0\mathbf{M}\times\mathbf{n}_\mathrm{i})\right)\cdot\mathbf{w}_a\,\mathrm{d}\Gamma_\mathrm{ai} = \\ \int_{\Omega_\mathrm{i}}\mathbf{M}\cdot\mathrm{curl}\mathbf{w}_\mathrm{a}\,\mathrm{d}\Omega_\mathrm{i}\end{aligned} \tag{10}$$

with $a = 1, 2, 3$. It is shown in [12] that the continuity condition of $\mathbf{H}_\mathrm{t}$, i.e.,

$$\begin{aligned}\frac{1}{\mu_0}\,(\mathrm{curl}\,\mathbf{A}^\mathrm{FEM} - \mu_0\mathbf{M})\times\mathbf{n}_\mathrm{i} + \\ \frac{1}{\mu_0}(\mathrm{curl}\,\mathbf{A}^\mathrm{BEM})\times\mathbf{n}_\mathrm{a} = 0\end{aligned} \tag{11}$$

on the boundary between iron and air is equivalent to

$$\frac{\partial\mathbf{A}^\mathrm{FEM}}{\partial n_\mathrm{i}} - (\mu_0\mathbf{M}\times\mathbf{n}_\mathrm{i}) + \frac{\partial\mathbf{A}^\mathrm{BEM}}{\partial n_\mathrm{a}} = 0, \tag{12}$$

where $\mathbf{n}_\mathrm{i}$ is the normal vector on Γ_ai pointing out of the FEM domain and $\mathbf{n}_\mathrm{a}$ is the normal vector on Γ_ai pointing out of the BEM domain. The boundary integral term on the boundary between iron and air Γ_ai in (10) serves as the coupling term between the BEM and the FEM domain.

By definition, the BEM domain contains no iron, and therefore $\mathbf{M} = 0$ and $\mu = \mu_0$. Eq. (8) then reduces to

$$\nabla^2\mathbf{A} = -\mu_0\mathbf{J} \tag{13}$$

As Cartesian coordinates are used eq. (13) decomposes into three scalar Poisson equations to be solved. For an approximate solution of these equations, the weighted residual is forced to zero and the weighting functions are chosen as the fundamental solution of the Laplace equation, which is in 3D

$$w = u^* = \frac{1}{4\pi R}. \tag{14}$$

With $\frac{\partial w}{\partial n_a} = q^* = -\frac{1}{4\pi R^2}$ and $\nabla^2 w = -\delta(R)$ we get the Fredholm integral equation of the second kind:

$$\frac{\Theta}{4\pi} A + \oint_{\Gamma_{ai}} Q_{\Gamma_{ai}}\, u^*\, \mathrm{d}\Gamma_{ai} + \oint_{\Gamma_{ai}} A_{\Gamma_{ai}}\, q^*\, \mathrm{d}\Gamma_{ai} = \int_{\Omega_a} \mu_0 \mathrm{J} u^*\, \mathrm{d}\Omega_a. \quad (15)$$

As it is common practice in Literature on boundary element techniques, e.g., [10] the notation u^* for weighting functions are used in eq. (15). The right hand side of eq. (15) is a Biot-Savart-type integral for the source vector potential A_s.

The components of the vector potential $\mathbf{A}$ at arbitrary points $\mathbf{r}_0 \in \Omega_a$ (e.g. on the reference radius for the field harmonics) has to be computed from 15 as soon as the components of the vector potential $\mathbf{A}_{\Gamma_{ai}}$ and their normal derivatives $\mathbf{Q}_{\Gamma_{ai}}$ on the boundary Γ_{ai} are known. Θ is the solid angle enclosed by the domain Ω_a in the vicinity of $\mathbf{r}_0$.

For the discretization of the boundary Γ_{ai} into individual boundary elements $\Gamma_{ai,j}$, C^0-continuous, isoparametric 8-noded quadrilateral boundary elements are used. They have to be consistent with the elements from the FEM domain touching this boundary. The discrete analogue of the Fredholm integral equation can be obtained by successively putting the evaluation point $\mathbf{r}_0$ at the location of each nodal point $\mathbf{r}_j$. This procedure is called point-wise collocation and yields a linear system of equations, The discrete analogon of equation 15 gives exactly the missing relationship between the Dirichlet data $\{\mathbf{A}_{\Gamma_{ai}}\}$ and the Neumann data $\{\mathbf{Q}_{\Gamma_{ai}}\}$ on the boundary Γ_{ai}.

Fig. 3 shows the relative multipole field components at 17 mm ref. radius as a function of the longitudinal position in the LHC main dipole extremity (comp. fig 1).

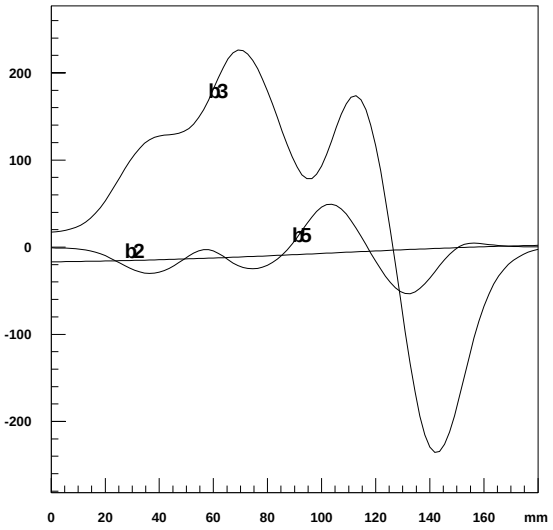

FIG. 3. Relative multipole field components at 17 mm ref. radius as a function of the longitudinal position in the LHC main dipole extremity. Zero is the end of the straight section.

VI. PERSISTENT CURRENTS

Field variations in the LHC superconducting magnets, e. g. during the ramping of the magnets, induce magnetization currents in the superconducting filaments that do not decay, but persist due to the lack of resistivity. The relative field errors created by these persistent currents are small in case of nominal field but become dominant at low excitation levels.

The calculation method for the persistent currents is based on a semi-analytical hysteresis model [40] for hard superconductors combined with the BEM-FEM method. The hysteresis model depends on a $J_c(B)$ current fit [9] and an extended Bean model [5], [42] for the superconducting filaments. The feed-back of the superconducting filament magnetization and the iron magnetization effects are calculated by means of an iterative scheme presented in [40]. This allows the calculation of multipole components as a function of the excitation and the powering cycle, and for arbitrarily shaped iron parts with non-linear B(H) curves.

Fig. 4 shows the relative multipole field components at 17 mm ref. radius as a function of the excitation between injection and nominal field level for the MQM insertion region quadrupole (including iron saturation and persistent current multipoles).

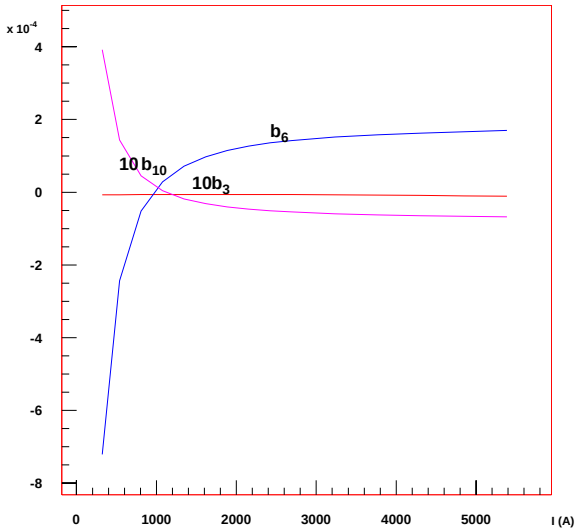

FIG. 4. Relative multipole field components at 17 mm ref. radius as a function of the excitation between injection and nominal field level for the MQM insertion region quadrupole (including iron saturation and persistent current multipoles) Ref. fig. 2.

VII. QUENCH ANALYSIS

Studying the magnet behavior in the event of transition to the resistive state (quench) is an important consideration during the design phase of SC magnets. The aim of these studies is to know whether or not the magnet is self-protected against resistive transitions, and how it can be protected in case the quenches threaten the integrity of the magnet.

For the case of long magnets with quench heaters the propagation effect can be neglected and an analytical model can be used for the calculation of the hot spot temperature. The basic equation that links the temperature of the conductor with the current is given by the heat balance equation under adiabatic conditions (no heat conduction and no cooling) [42]

$$R\,I(t)^2 = C(T)\,V\,\frac{dT}{dt}, \tag{16}$$

$$\frac{\rho_{Cu}(B(I),T,RRR)}{A_{Cu}}\,l\,I(t)^2 = C(T)\,A_T\,l\,\frac{dT}{dt}, \tag{17}$$

$$\frac{dT}{dt} = \frac{I(t)^2\rho_{Cu}(B(I),T,RRR)}{A_{Cu}A_T C(T)}, \tag{18}$$

where A_{Cu} is the copper cross-section of a conductor, A_T the total cross-section of the conductor, $C(T)$ the average specific heat (in units of $\frac{J}{kgK}$) of the conductor, and $\rho_{Cu}(B(I),T,RRR)$ is the resistivity of the copper as a function of magnetic field, temperature and the residual resistivity ratio (i.e., the ratio between copper resistivity at 293 K and at 4.2 K in absence of magnetic field). The argument of ρ_{Cu} is subsequently omitted. l is the length of the magnet. Separation of variables and integration yields

$$\int_0^\infty I(t)^2 dt = A_{\rm Cu}A_{\rm T}\int_{T_0}^{T_{\rm max}}\frac{C(T)}{\rho_{Cu}}dT. \tag{19}$$

The term on the left hand side of eq. (19), i.e., the time integral over the square of the current, is usually expressed in units of 10^6 A^2 s and is called MIIT. The MIITs represent the quench load. The term on the right hand side of eq. (19) represents the quench capacity of a given SC cable. From this equation the map of temperature T in the coils as a function of time can be evaluated.

It is assumed that a quench starts in the high field region of the outer layer dipole coil at the nominal current of 11800 A and propagates longitudinally and transversally to the neighboring turns. The initial longitudinal quench velocity is 15-20 m/s in the outer layer, and the transition propagates transversally with a turn-to-turn delay of 20-25 milliseconds (values according to measurements). The transverse propagation is limited by the insulation and the helium content in the cable. The magnet is protected by strip heaters covering the full length of 5+8 turns per pole in the outer layer shells. The idea is to warm up sufficiently large sections of the coil in order to spread out the stored magnetic energy. The quench heaters are effective after a delay of about 50 milliseconds from the onset of the quench. Since the magnet is by-passed through a cold diode, the coils will dissipate the full energy stored in the magnet. The bulk of the magnet acts as a current source for the quenching part of the magnet.

If we neglect the voltage and temperature rise due to the quench propagation, i.e., assume that the resistivity created by the initial quench is too low to produce a significant decrease of the current, then a 2D analytical model can be used to calculate the current evolution in the magnet. In this case we assume that the current evolution is controlled by the resistance of the turns under the strip heaters. As the heaters cover the entire length of the magnet, the problem can be treated as a 2D field problem. The time dependence of the current is given by

$$\frac{dI}{dt} = \frac{U}{L} - \frac{I\,R}{L}, \tag{20}$$

where R is the total resistance of all conductors quenched by the strip heaters, U is the armature voltage and L is the self inductance of the magnet. The value of the resistance is given by

$$R = \sum_{i=1}^{N} 8l\frac{\rho_{Cu}}{A_{\rm Cu}}u(t-t_{\rm qi}), \tag{21}$$

where the $t_{\rm qi}$ are the heater delays of the protection system for each of the N conductors and $u(t)$ is the unitary step function. The factor 8 comes from the series connections of the turns in the two-in-one magnets. The hot spot temperature can be evaluated by solving a set of $N+2$ ordinary (first-order) differential equations (T_0 is the temperature of the conductor in which the quench is initiated, T_i $(i=1,...,N)$ are the temperatures of the conductors covered by the quench heaters):

$$\frac{dT_0}{dt} = \frac{I^2\rho_{Cu}}{A_{Cu}A_T C(T_0)}, \tag{22}$$

$$\frac{dT_i}{dt} = \frac{I^2\rho_{Cu}}{A_{Cu}A_T C(T_i)}u(t-t_{\rm qi}), (i=1,...,N) \tag{23}$$

$$\frac{dI}{dt} = \frac{U}{L} - \frac{I}{L}\sum_{i=1}^{N} 8l\frac{\rho_{Cu}}{A_{\rm Cu}}u(t-t_{\rm qi}). \tag{24}$$

Notice that the conductivity of the copper ρ_{Cu} in conductor i depends on the temperature and the local magnetic field in the coil (B_i, T_i). The length l of the magnet cancels if the inductance is given per unit length. The system of differential equations is solved using the Runge-Kutta method.

Fig. 5 gives the time evolution of the current, resistivity and temperature for a quench that is assumed to originate in the innermost (pole) turn of the outer layer of the coil. The 4th order Runge-Kutta method was used with a fixed step size of 0.001 sec. The maximum temperature is

314 K, the MIITs integral yields $\int_0^\infty I(t)^2 dt = 0.312 \cdot 10^8$ A^2 s.

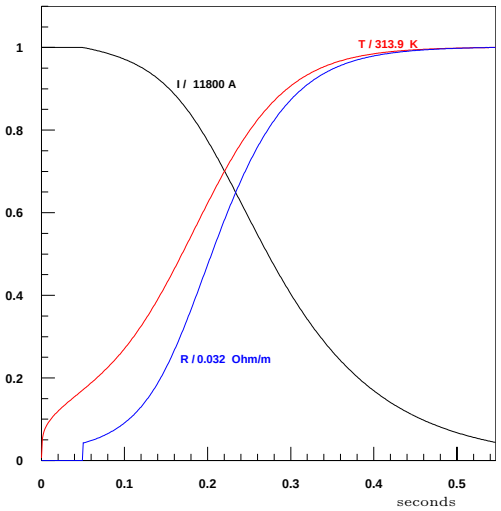

FIG. 5. Time evolution of the current, resistivity and temperature (normalized) for a quench that is assumed to originate in the pole turn of the outer layer of the LHC main dipole.

VIII. MATHEMATICAL OPTIMIZATION

Mathematical optimization techniques have for decades been applied to computational electromagnetics. Halbach [16] introduced in 1967 a method for optimizing coil arrangements and pole shapes of magnets by means of finite-element field calculation. Armstrong, et. al. [3] combined in 1982 optimization algorithms with the volume-integral method for the pole profile optimization of an H-magnet. These attempts tended to be application-specific, however. Only since the late 1980s, have numerical field calculation packages for both 2D and 3D applications been placed in an optimization environment. Reasons for this delay have included constraints in computing power, problems with discontinuities and non-differentiabilities in the objective function arising from FE-meshes, accuracy of the field solution, and software implementation problems.

Application of mathematical optimization techniques to magnet design using numerical field computation causes special requirements on the optimization method because of the following reasons.

- The computing time for each objective function evaluation can be in the range of hours (DEC-Alpha-station 600). The time for the evaluation of the next search point can therefore be neglected.
- As the objective functions are calculated through FEM procedures, they are covered in numerical errors. This makes the application of gradient methods problematic if differential quotients for the gradient approximation have to be used.
- As the objective functions are not defined explicitly, continuity, differentiability and convexity have to be *assumed* for the application of some classes of optimization methods.
- Some of the trial solutions might lead to physically meaningless structures and the crash of finite element calculations. This has to be considered during the set-up of the parametric model.
- Magnet design has to deal with multiple (conflicting) objectives.

Most of the real-world optimization problems (including the design of SC magnets) involve multiple conflicting objectives. In our case, for example, the search for a maximum main field and a small volume of superconductor material. There is also a payoff between a maximum field and small saturation induced field errors. Characteristic of these *vector-optimization* problems is the appearance of an objective-conflict in which the individual solutions for each single objective function differ and no solution exists where all the objectives reach their individual minimum. The procedures for solving vector-optimization problems consist of three different parts: decision making, treatment of constraints, and optimization algorithm. Optimization procedures specially suited for magnet design have been extensively described in author's papers, e.g. [31].

From the beginning, the ROXIE program has been structured to allow for the application of mathematical optimization techniques. Numerous methods are available for decision making and the treatment of nonlinear constraints. These can be combined with optimization algorithms where both search routines (not using the derivative of the objective function) and higher order methods are available. All the evaluated field quantities can be addressed as objectives for the optimization. Decision making methods include objective weighting, distance function, constraint formulation (Marglin method) and the automatic set-up of payoff tables. Nonlinear constraints can be treated either by a feasible domain method, the penalty transformation or the Augmented-Lagrangian function. The following optimization algorithms are available:

- EXTREM (search routine, suited for most of the problems including objective weighting functions and penalty functions.
- Levenberg-Marquard (first order method, specially suited for inverse field computations i.e. the minimization of a least squares objective function) [3]
- Davidon- Fletcher- Powell (Quasi- Newton method specially suited for Lagrange- Multiplier estima-

tion). The sensitivity analysis with Lagrange multiplier estimation allows to find the hidden resources of a particular design, as the Lagrange multipliers are a measure for the price which has to be paid when a particular objective is to be improved.

- Genetic algorithms which are applied for the conceptual design of magnets [5].
- A speedup scheme using artificial neural networks (ANN) for the approximation of the objective function.

IX. GENETIC OPTIMIZATION

Genetic optimization algorithms were developed in the mid 1970s by Holland [18]. Evolution strategies which go back to Darwin's work and which are based on the link between reproductive populations rather than genetic links were independently developed by Schwefel [34] and Rechenberg [32]. Facilitated by the development of computing power, both evolution strategies and genetic algorithms have been given considerable attention lately and have been applied to problems in electromagnetic field computation [38]. The different design parameters are combined by linear sampling of the floating point parameters

$$\Delta x_i \in [0, x_{i\max} - x_{i\min}] \tag{25}$$

and Gray-coding of the resulting binaries into a bit-string (chromosome). With binary coding, two neighbouring integers, e.g., 7 (0111) and 8 (1000) differ considerably in the bit string, or in other words, their Hamming-distance (number of different bits) is larger than one. The applied *Gray-coding* ensures that neighboring integers differ by one bit only.

Genetic optimization algorithms are driven by the following main operators:

- Crossover, a recombination of strings of two chromosomes by breakage at a random point and reunion of the alleles. This is the underlying mechanism of sexual reproduction.
- Mutation is the process of an alteration in a chromosome structure. In optimization, this process avoids preliminary convergence towards a local minimum.
- Selection is the force behind changes in the genotype in populations through differential reproduction, i.e., less fit members of the population having a smaller mating probability.

Selection methods can be divided into the following different groups:

- Fitness proportional (Fairy-Wheel) selection: A fitness value that represents a probability for selection is assigned to each of the chromosomes

$$F(x_i) = \frac{f(x_i)}{\sum_{j=1}^{n} f(x_j).} \tag{26}$$

- Niching selection: Niching methods introduce a concept of distance according to the observation that a population spread over a geographic range will become genetically differentiated in a number of sub-environments, so-called niches. The new offspring replaces the chromosome which is closest in parameter space (or has the smallest Hamming-distance on the bit level) if its objective function value (fitness) is lower.

Whereas with fairy-wheel selection the whole population is subject to a fitness ranking, the selection in the niching genetic algorithm is performed on the level of each individual. Selected chromosomes are then immediately joined to the population.

The effect of the niching method is that *a number* of local optima are found which can then be further investigated and compared.

X. OPTIMIZATION SPEED-UP USING A NEURAL NETWORK APPROXIMATOR

Neural networks have been applied in recent years to the design optimization in computational electromagnetics. Serving as universal approximators to solve "best fit" problems, Feed Forward Back-Propagation Neural Networks were successfully applied to the solution of inverse optimization problems, whereas Radial Basis Function (RBF) Neural Networks were used to speed-up optimization algorithms [2], [15]. In the ROXIE program a RBF Neural Network is used to speed up deterministic optimization algorithms.

Radial basis function neural networks (RBF) are two-layer feed-forward networks with radial basis functions as activation functions in the hidden units and linear activation functions in the output units. For the approximation of the objective function an RBF neural network with p inputs and one output can be used. The RBF network approximates the mapping f by a linear combination

$$O(x) = w_0 + \sum_{i=1}^{n} w_i \phi_i(x), \tag{27}$$

where each of the n hidden units is activated with a Gaussian radial basis function

$$\phi_i(x) = \exp(-||c_i - x||^2/(2\sigma_i^2). \tag{28}$$

In out application, the centers c_i are chosen as the data points of the training set $\mathbf{Z} = \{x_j, t_j\}_{j=1}^{n}$ and the widths

σ_i are set to a fraction of the training set diameter. The crucial part of the training is the determination of the weight vector $\mathbf{w} = [w_0, \ldots, w_n]$ as a solution of the regularized least square problem

$$\min_{\mathbf{w}}\{||\mathbf{\Phi w} - \mathbf{t}|| + \lambda^2||\mathbf{w}||\}, \tag{29}$$

where $\mathbf{\Phi}$ is an interpolation matrix, $\mathbf{t}$ is a target vector and λ is a regularization parameter [36] The use of RBF neural network as an approximator is motivated by its two main advantages: A good local approximation quality and a small computational effort for the learning algorithm compared to the objective function evaluation (BEM-FEM calculation).

The speed-up scheme is based on the observation that deterministic search algorithms do perform trials into the regions already visited in previous iterations. A time-consuming objective function evaluation can then be replaced by a RBF approximation. This leads to the following algorithm, [4]:

1. Perform some initial steps with the search algorithm.
2. Generate a new search point x and a training set $\mathbf{Z}$ from previous trials.
3. Investigate, if a reliable RBF approximation can be constructed in point x:
   (a) If the point x is in the "reliable" region of the search domain, then train the RBF neural network. If the network was successfully trained, then evaluate the approximation $\tilde{f}(x)$ and substitute $f(x^{(i)}) \leftarrow \tilde{f}(x^{(i)})$.
   (b) If the point x is not in the reliable region, or the network cannot be trained successfully, then evaluate $f(x)$ by means of a numerical field computation.
4. Goto 2 until convergence.

The speed-up which could be achieved in magnet optimization is in the range of 20 %.

XI. SUMMING UP: THE INTEGRATED DESIGN PROCESS

The modeling capabilities of the ROXIE program together with its interfaces to CAD and CAM and the mathematical optimization routines have inversed the classical design process where numerical field calculation is performed for only a limited number of numerical models (more or less) resembling the engineering design. ROXIE is now more and more used as an approach towards an integrated design of SC magnets [2] starting as early as the conceptual phase using genetic algorithms [5]. The interfaces then allow the making of drawings according to the computer models in considerable less time than before. The steps of the integrated design process for superconducting magnets are as follows:

- Feature-based geometry modeling of the coil and yoke, both in two and three dimensions using only a number of meaningful input data to be supplied by the design engineer. This is a prerequisite for addressing these data as design variables of the optimization problem.
- Conceptual design using a genetic algorithm, which allows the treatment of combined discrete and continuous problems (e.g. the change of the number of conductors per block) and the solving of material distribution problems. The applied niching method supplies the designer with a number of local optima which can then be studied in detail.
- Subject to a varying magnetic field, currents that screen the interior of the SC filaments are generated in their outer region. The relative field errors caused by these currents are highest at injection field level and have to be calculated to allow a subsequent part-compensation by geometrical field errors. Deterministic search algorithms are used for the final optimization of the coil cross-section.
- Minimization of iron-induced multipoles using a finite-element method with a reduced vector-potential formulation .
- Calculation of the peak voltage and peak temperature during a quench.
- Sensitivity analysis of the optimal design through Lagrange-multiplier estimation and the set-up of payoff tables. This provides an evaluation of the hidden resources of the design.
- Tolerance analysis calculating Jacobian-Matrices and estimation of the standard deviation of the multipole field errors.
- 3D coil-end geometry and field optimization including the modeling and optimization of the asymmetric connection side, ramp and splice region and external connections.
- 3D field calculation of the saturated iron yoke using the method of coupled boundary/finite-elements, BEM-FEM.
- Production of drawings by means of a DXF interface for both the cross-sections and the 3D coil-end regions.
- End-spacer design and manufacture by means of interfaces to CAD/CAM (DXF, VDA), rapid prototyping methods (laser sinter techniques), and computer controlled 5-axis milling machines.
- Tracing of manufacturing errors from measured field imperfections, i.e., the minimization of a least-squares error function using the Levenberg-Marquard optimization algorithm.

[1] M. Aleksa, S. Russenschuck, C. Völlinger: Parametric Quadrilateral Meshes for the Design and Optimization of Superconducting Magnets, ICAP2000, Darmstadt, Germany

[2] P. Alotto, A. Caiti, G. Molinari, M. Repertto: Multiquadratics-based algorithm for the acceleration of Simulated Annealing Optimization Procedure , IEEE Trans. on Magnetics, Vol. 30, pp. 2929-2939, 1994.

[3] Armstrong, A.G.A.M. , Fan, M.W., Simkin, J., Trowbridge, C.W.: Automated optimization of magnet design using the boundary integral method, IEEE Transactions on Magnetics, 1982

[4] Bazan M., Russenschuck S.: Using neural networks to speed-up optimization algorithms , submitted for publication in European Physical Journal.

[5] Bean, C.P.: Physics review letters, 1962

[6] T. Beier et al., Feature-based image metamorphosis , Computer Graphics 26(2), 1992.

[7] T.D. Blacker et al., Paving: A new approach to automated quadrilateral mesh generation. Int. J. Numer. Method. Eng., 32:811-847, 1991.

[8] Biro, O., Preis, K.: On the use of the magnetic vector potential in the finite-element analysis of three-dimensional eddy currents, IEEE Transactions on Magnetics, 1989

[9] Bottura, L.: A Practical Fit for the Critical Surface of NbTi, 16th International Conference on Magnet Technology, Florida, USA, 1999.

[10] Brebbia, C.A.: The boundary element method for engineers, Pentech Press, 1978.

[11] Cohon, J.L.: Multiobjective Programming and Planning, Academic Press, New York, 1978

[12] Fetzer, J.: Die Lösung statischer und quasistationärer elektromagnetischer Feldprobleme mit Hilfe der Kopplung der Methode der finiten Elemente und der Randelementmethode, Fortschritt Berichte VDE, Reihe 21, VDE Verlag, 1992

[13] E. Gröller, Interactive transformation of 2d vector data , Technical University Vienna, Institute for Computer Graphics.

[14] T. Ishikawa, M. Matsunami: An optimization method base on radial basis functions , IEEE Transactions on Magnetics, Vol. 33, pp. 1868-1871, 1997.

[15] Th. Ebner, Ch. Magele, B. R. Brandstätter, K. R. Richter: Utilizing Feed Forward Neural Networks for Acceleration of Global Optimization Procedures IEEE Transactions on Magnetics, Vol. 34, pp. 2928-2931, 1998.

[16] Halbach, K.: A Program for Inversion of System Analysis and its Application to the Design of Magnets, Proceedings of the International Conference on Magnet Technology (MT2), The Rutherford Laboratory, 1967

[17] Halbach, K., Holsinger R.: Poisson user manual, Techn. Report, Lawrence Berkeley Laboratory, Berkeley, 1972

[18] Holland, J.H.: Genetic algorithms, Scientific American, 1992

[19] Hornsby, J.S.: A computer program for the solution of elliptic partial differential equations, Technical Report 63-7, CERN, 1967

[20] Jacob, H.G.: Rechnergestützte Optimierung statischer und dynamischer Systeme, Springer, 1982.

[21] M. Karppinen, S. Russenschuck, A. Ijspeert: Automated Design of a Correction Dipole magnet for LHC Epac 96, LHC Project Report 29, 1996, CERN, Geneva

[22] Kuester, J., Mize, J.H.: Optimization techniques with Fortran , Mc Graw-Hill, 1973

[23] Kuhn, H.W., Tucker, A.W.: Nonlinear Programming, Proceedings of the 2nd Berkeley Symposium on Mathematical Statistics and Probability, University of California, Berkeley, 1951

[24] Kurz, S., Russenschuck, S.: Accurate Calculation of Magnetic Fields in the End Region of Superconducting Accelerator Magnets using the BEM-FEM Coupling Method, PAC99, New-York

[25] Kurz, S., Russenschuck, S., Siegel, N.: Accurate calculation of fringing fields in the LHC main dipoles, Sixteenth International Conference on Magnet Technology, MT16, Fl, USA, 1999.

[26] S. Kurz et al., The application of the BEM-FEM coupling method for the accurate calculation of fields in superconducting magnets, Electrical Engineering, 1999.

[27] Mahfoud, S.W.: Niching Methods for Genetic Algorithms, PhD thesis, University of Illinois, Urbana-Champaign, 1995

[28] G.D. Nowottny, Netzerzeugung durch Gebietszerlegung und duale Graphenmethode , Shaker Verlag, Aachen, 1999.

[29] C. Paul, K. Preis, S. Russensschuck: 2d FE-Calculation of Superconducting Magnets Applying a Reduced Vector Potential A_r- Formulation 7th International IGTE Symposium Graz, Austria, 1996, LHC Project Report 77

[30] S. Ramberger, S. Russenschuck: Genetic algorithms with niching for conceptional design studies , COMPUMAG, Rio, 1997

[31] S. Russenschuck: Pareto-optimization in Computational Electromagnetics International Journal of Applied Electromagnetics in Materials 4, Elsevier, 1993, Divisional Report AT/92-27, LHC-Note 205, CERN, Geneva

[32] Rechenberg, I.: Evolutionsstrategie: Optimierung technischer Systeme nach Prinzipien der biologischen Evolution, Frommann Verlag, 1973

[33] S. Russenschuck et al.: ROXIE: Routine for the optimization of magnet x-sections, inverse field calculation and coil end design , CERN 99-01.

[34] Schwefel, H.P.: Numerische Optimierung von Computer-Modellen mittels der Evolutionsstrategie, Birkhäuser Verlag, 1977

[35] Stadler, W.: Preference optimality and application of Pareto-optimality in Marzollo, Leitmann: Multicriterion Decision Making, CISM Courses and Lectures, Springer, 1975

[36] A. N. Tikchonov, V. Y. Arsenin: Solution of Ill-Posed Problems , V. H. Winston, Washington.

[37] J.F. Thompson et al., Aspects of numerical grid generation: current science and art. , Technical report, American Institute of Aeronautics and Astronautics, Washing-

ton, D.C. 20024 USA, 1993.
[38] Uler, G.F., Mohammed, O.A., Koh, C.S.: Design optimization of electrical machines using genetic algorithms, IEEE Transactions on Magnetics, 1995
[39] Völlinger, C.: Modified Bean model and FEM combined for the calculation of persistent currents in superconducting coils, 9th IGTE Symposium, Sept. 11-14, 2000, Graz.
[40] Völlinger, C.: Modified Bean model and FEM combined for the calculation of persistent currents in superconducting coils, 9th IGTE Symposium, Sept. 11-14, 2000, Graz.
[41] Winslow A.A.: Numerical solution of the quasi-linear Poisson equation in a non-uniform triangular mesh, Jorunal of computational physics, 1, 1971
[42] Wilson, M.N.: Superconducting Magnets, Oxford Science Publications, 1983